

Final Report

*Award H-74B: Characterization of the spatial distribution of
particulate concentration and properties during TexAQS-II*

Prepared by:

Don R. Collins

Texas A&M University
Department of Atmospheric Sciences
1204 Eller O&M Bldg / 3150 TAMU
College Station, TX 77843-3150

Prepared for:

Houston Advanced Research Center
4800 Research Forest Drive
The Woodlands, TX 77381

August 2007

Table of Contents

Executive Summary	2
Sampling Locations and Timeline	4
Experimental Approach	6
Data Analysis and Results	7
Project webpage	8
Study-averaged distributions and complete time series	9
Calculated data products	14
Comparison of calculated mass concentrations with TCEQ TEOM measurements.....	16
Evidence of contribution of sea salt to PM2.5	17
Dependence of particulate properties on back trajectory	21
References.....	22
Appendix I - Formats used in data files	23

Executive Summary

The objective of this research project was to quantify the spatial distribution of the size-resolved concentration and hygroscopicity of particulates in the Houston area. Three identical instruments were operated at the Aldine, Deer Park, and Bayland Park TCEQ monitoring sites. These measurements were coordinated with those of an array of gas and particulate properties made by other researchers supported by HARC. Specifically, the research group from Pacific Northwest National Laboratory led by Carl Berkowitz measured size-resolve particulate composition and the concentrations of gas phase O_3 , NO_x , CO , and a range of organics, while Renyi Zhang and his research group used a proton transfer reaction mass spectrometer to make high time resolution measurements of several organic compounds. The sampling period extended from September 7th through 27th. Beyond characterization of the spatial variability and evolution of particulate concentration and properties, these measurements provide details of the liquid water content present in that particulate population, which is needed to estimate the conversion rate of N_2O_5 to HNO_3 , both of which were concurrently measured.

Tandem differential mobility analyzers (TDMAs) similar to those used to examine particle size distributions and hygroscopicity in the Houston area during a number of prior studies (e.g., Gasparini et al., 2004) were operated continuously at the three sites identified above. Over a period of 30-45 minutes, these instruments cycle through a fixed sequence of measurements. Each of the instruments was automatically calibrated every night and more extensive calibrations were conducted prior to, once during, and following the experiment. Confidence in the accuracy of the dataset was gained through comparison of hourly-averaged mass concentrations calculated from the size distributions measured with the TDMA and directly measured by TCEQ using TEOMS. As is evident from the measurement time series provided in this report, data collection was largely uninterrupted during the project. All measured distributions and generated products are provided graphically and in ascii format through a user-friendly project website at the URL identified in the report. The following are several salient findings from the project:

- Variability among the sites in size-resolved properties was rather limited despite the significant differences in local emissions sources. The size-dependent trend in hygroscopicity observed at each of the locations suggests the aerosol is largely an external mixture (multiple particle types present) with the more hygroscopic, sulfate-dominated, mode reaching a peak fractional contribution at roughly $0.2 \mu m$.
- The hygroscopicity of the 0.05 to $0.4 \mu m$ diameter particles appears to vary over longer timescales, sometimes exceeding a day, while that of the smaller particles exhibits little day-to-day variability, but instead has a pronounced diurnal pattern that reflects increased importance of sulfuric acid condensation during the afternoon and of secondary organic aerosol at night.
- The impact of mobile emissions of primary aerosols during morning rush hour is evident in the size distributions of the insoluble component of the particulates determined for all three sites. The insoluble particulate concentrations then decrease during the afternoon as the boundary layer depth increases.
- Peak concentrations in the size distributions of the soluble component of the particulates are observed in mid-afternoon during peak photochemical activity. Production of secondary sulfates during this time is pronounced in the number size distributions, but has a relatively modest impact on the resulting mass concentrations.

- There is strong evidence that sea salt contributed as much as $15 \mu\text{g}/\text{m}^3$ to the total $\text{PM}_{2.5}$ during a multi-day episode in August, which emphasizes the importance of this often overlooked particle type in coastal regions.
- At each of the three sites, the hygroscopicity of the dominant $0.2 \mu\text{m}$ diameter particle population was greater when the sampled air came from the south than when from the east, and greater when from the east than from the north. This variation in hygroscopicity likely reflects the organic fraction of these larger particles.
- Hygroscopic growth factor distributions for the $0.6 \mu\text{m}$ particles indicate a significant and only weakly origin-dependent contribution of dust or some other primary particle type.

These measurements must be evaluated together with the complementary datasets generated during the TexAQS-II study period. Assessment of the ability of current air quality models to reproduce the particulate concentration and inferred composition will aid in evaluating emissions reductions needed to reduce area $\text{PM}_{2.5}$ if Houston becomes non-compliant. Among the analyses that could improve modeling accuracy, and subsequently SIP effectiveness, are testing model predictive skill at the following:

Model prediction	Calculated from measured size and hygroscopicity distributions
Primary particulate concentration	Primary particle-only size distribution determined as product of size-resolved fraction of particles in non-hygroscopic modes from TDMA distributions and size-resolved particle concentration from DMA distributions
Contribution of sea salt to $\text{PM}_{2.5}$	Sea salt-only size distribution determined as product of size-resolved fraction of particles in very hygroscopic modes from TDMA distributions and size-resolved particle concentration from DMA distributions
Impact of condensation of secondary inorganics (primarily sulfate) and organics on particle size distribution and overall $\text{PM}_{2.5}$	Rate at which median diameter of size distribution modes increase, coupled with rate at which hygroscopicity of the particles in those modes changes
Flux of $\text{PM}_{2.5}$ across Houston metropolitan boundary	Lidar retrieved vertical $\text{PM}_{2.5}$ as determined using CALIPSO backscattering profiles and $\text{PM}_{2.5}$ to backscattering ratio calculated using size and hygroscopicity distributions

Sampling locations and timeline

Identical instruments combining differential mobility analyzers (DMAs) and tandem differential mobility analyzers (TDMAs) were operated at each of the three Houston Triangle sites identified on the map in Figure 1. These instruments were used to continuously measure the size distribution and size-resolved properties of the particulates. The first full day of sampling was on September 11 and the last full day was on October 2. The calendar presented in Figure 2 identifies which of the three instruments were operational on each of the project days and provides some meteorological context through the calculated back trajectories. The trajectories were calculated using Hysplit for arrival at each of the three sites at local noon. To clearly show the features in the trajectory graph pairs, a full-size version of the graphs for September 21 is shown in Figure 3.



Figure 1. Map showing the locations of the three TCEQ sampling sites.

Sunday	Monday	Tuesday	Wednesday	Thursday	Friday	Saturday
	Sep 11 Bayland Park	Sep 12 Bayland Park Deer Park	Sep 13 Bayland Park Deer Park	Sep 14 Aldine Bayland Park Deer Park	Sep 15 Aldine Bayland Park Deer Park	Sep 16 Aldine Bayland Park Deer Park
Sep 17 Aldine Bayland Park Deer Park	Sep 18 Aldine Bayland Park Deer Park	Sep 19 Aldine Bayland Park Deer Park	Sep 20 Aldine Bayland Park Deer Park	Sep 21 Aldine Bayland Park Deer Park	Sep 22 Aldine Bayland Park Deer Park	Sep 23 Aldine Bayland Park Deer Park
Sep 24 Aldine Bayland Park Deer Park	Sep 25 Aldine Bayland Park Deer Park	Sep 26 Aldine Bayland Park Deer Park	Sep 27 Aldine Bayland Park Deer Park	Sep 28 Aldine Bayland Park Deer Park	Sep 29 Aldine Bayland Park Deer Park	Sep 30 Aldine Deer Park
Oct 1 Aldine Deer Park	Oct 2 Aldine Deer Park	Oct 3 Aldine Deer Park				

Figure 2. Calendar for project period identifying operational status and providing meteorological context for the measurements through the calculated back trajectories.

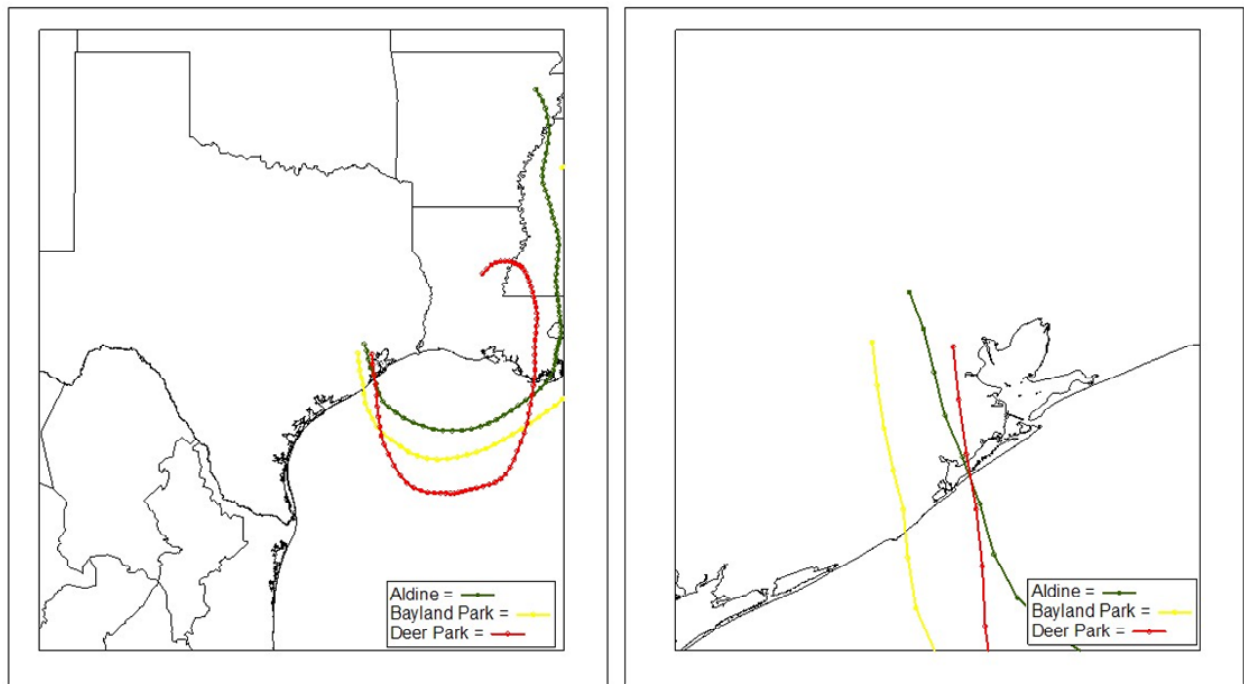


Figure 3. Full-size trajectory graphs for September 21.

Experimental Approach

A schematic of the DMA / TDMA system is shown in Figure 4. A thorough description of the various components within the DMA / TDMA is provided in *Gasparini et al. (2004)*. Two Aerosol Dynamics, Inc., High Flow Differential Mobility Analyzers (HF-DMAs; Stolzenburg et al., 1998) are used in the DMA / TDMA to maximize particle count rate. Flow rates, high voltages, and relative humidity are actively controlled through Labview-based proportional-integral-differential (PID) control algorithms. The DMA / TDMA system is mounted in a mobile frame as shown in the photograph in Figure 4.

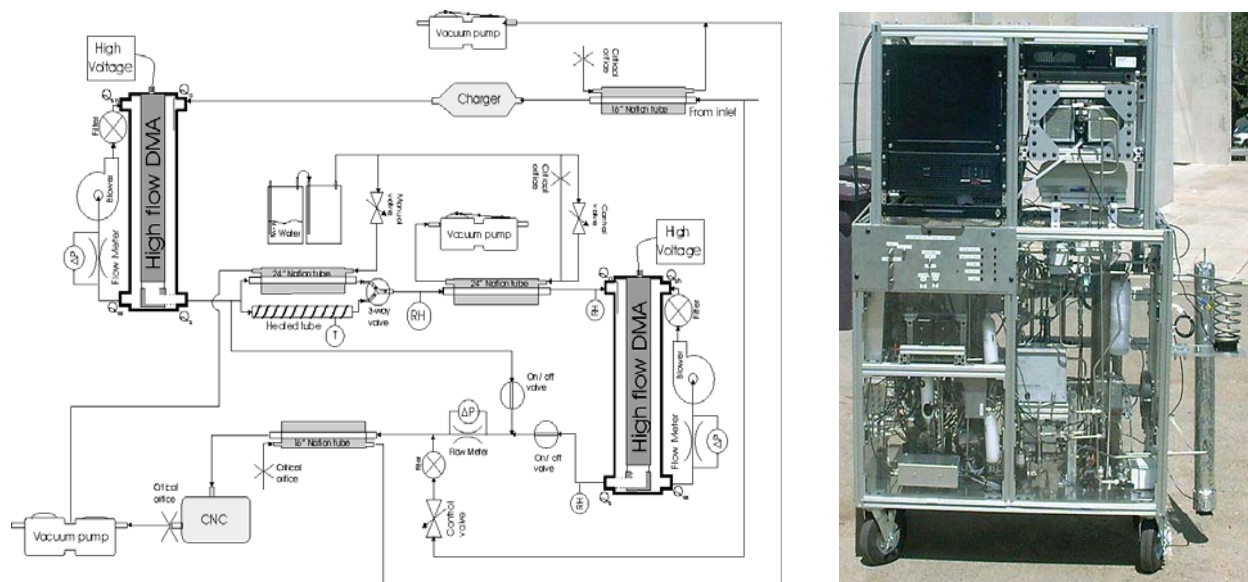


Figure 4. Schematic (left) and photograph (right) of the DMA / TDMA system used during this study.

A DMA separates particles within a narrow size range from an introduced polydisperse aerosol (Knutson and Whitby, 1975). The particle size separated is controlled by the flow rates through the instrument and by an applied high voltage. To measure a particulate size distribution, the applied voltage is varied stepwise or continuously to vary the particle size separated over time. During this mode of operation, the second DMA shown in Figure 4 is bypassed. Separated particles are detected using a condensation particle counter (CPC), which has a detection limit of approximately $0.01 \mu\text{m}$ diameter. The size-resolved ambient concentration is determined from the particle count rate through an inversion that accounts for particle transmission through the instrument and for the probability that particles possess charges of the appropriate polarity (*Collins et al., 2002*). The applied voltage is typically scanned over a period of approximately two minutes.

When measuring hygroscopic growth, the aerosol passes through both the first and second DMAs. Tandem differential mobility analyzers such as this have been employed extensively to characterize size-resolved hygroscopicity (*Liu et al., 1978; McMurry and Stolzenburg, 1989*). The aerosol is dried upon entering the instrument and the electric field in the first HF-DMA is held constant in order to select a monodisperse aerosol. The exiting monodisperse aerosol is then exposed to, and equilibrates with, an environment in which the

relative humidity is controlled to 85%. Following this exposure to high RH, the aerosol passes through the second DMA, in which the electric field is ramped up and then back down, and the resulting size- and hygroscopically-resolved aerosol is counted by the CPC. Hygroscopicity is described by the ratio of the diameter of a particle following exposure to high RH, D_p , to its initial dry diameter, D_p^* . This ratio is commonly referred to as the hygroscopic growth factor. For the measurements made at the Houston Triangle sites, particles having diameters of 0.013, 0.025, 0.050, 0.100, 0.200, 0.400, and 0.600 μm were analyzed. The blue rectangles in the number and volume size distribution graphs in Figure 5 show the location of the particle sizes at which hygroscopicity was measured. Measurement of one particle size continues until a minimum number of particles are counted or a maximum number of scans are completed. This results in measurement times that range from about two to ten minutes.

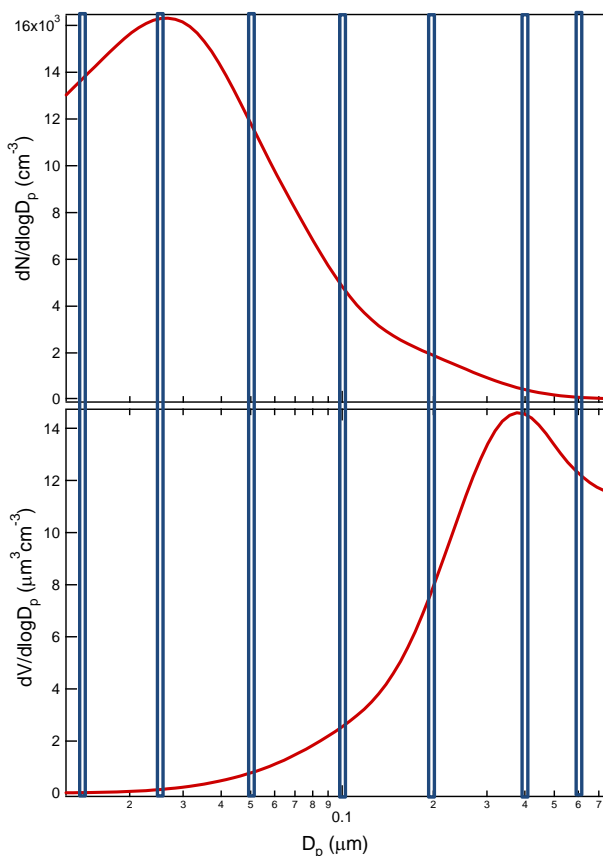


Figure 5. Number and volume size distributions used to highlight the particle sizes at which hygroscopicity was measured (blue rectangles).

Data Analysis and Results

As discussed above, the TDMA's were deployed to the Aldine, Bayland Park, and Deer Park sites between 7 and 11 September. Each of the instruments collected data continuously through 29 September (Bayland Park) or 3 October (Aldine and Deer Park). There were only brief unplanned interruptions in the operation of the three instruments. Each instrument was calibrated in the field during the last week of the study. Inspection of the data during and after the field intensive suggested that all three instruments functioned properly throughout the

campaign. All data collected through this project have been provided to HARC in a standard format that is described in Appendix I. These data have been inverted as described above and quality checked.

Project webpage

Much of our effort following the completion of the sampling component of the study was directed at generating the thousands of graphs intended to help us and other participants interpret and compare the data and at creating the project website through which these graphs would be linked. The focus on the latter is motivated by our experience during prior studies that simply making data available does not promote their integration with other measurements, which is essential for this type of collaborative project. The web interface to the data shown in Figure 6 has the URL

<http://www.met.tamu.edu/research/aerosol/Webpage/Houstontriangledata/September2006.html>

September 2006 ▶ Houston Triangle Data						
Sunday	Monday	Tuesday	Wednesday	Thursday	Friday	Saturday
27	28	29	30	31	1	2
3	4	5	6	7	8	9
10 Aldine d w txt Deer Park d w txt Bayland Park d w txt	11 Deer Park d txt Bayland Park d txt Trajectory	12 Deer Park d txt Bayland Park d txt Trajectory	13 Deer Park d txt Bayland park d txt Trajectory	14 Aldine d txt Deer Park d txt Bayland Park d txt Trajectory	15 Aldine d txt Deer Park d txt Bayland Park d txt Trajectory	16 Aldine d txt Deer Park d txt Bayland Park d txt Trajectory
17 Aldine d w txt Deer Park d w txt Bayland Park d w txt Trajectory	18 Aldine d txt Deer Park d txt Bayland Park d txt Trajectory	19 Aldine d txt Deer Park d txt Bayland Park d txt Trajectory	20 Aldine d txt Deer Park d txt Bayland Park d txt Trajectory	21 Aldine d txt Bayland Park d txt Trajectory	22 Aldine d txt Deer Park d txt Bayland Park d txt Trajectory	23 Aldine d txt Deer Park d txt Bayland Park d txt Trajectory
24 Aldine d w txt Deer Park d w txt Bayland Park d w txt Trajectory	25 Aldine d txt Deer Park d txt Bayland Park d txt Trajectory	26 Aldine d txt Deer Park d txt Bayland Park d txt Trajectory	27 Aldine d txt Deer Park d txt Bayland Park d txt Trajectory	28 Aldine d txt Deer Park d txt Bayland Park d txt Trajectory	29 Aldine d txt Deer Park d txt Bayland Park d txt Trajectory	30 Aldine d txt Deer Park d txt Trajectory

Study Averages	Time-resolved study averages
Bayland Park	Bayland Park
Deer Park	Deer Park
Aldine	Aldine

Figure 6. Front page of the generated project website.

Both the daily (d) and weekly (w) pages contain time series of the number size distribution, normalized number size distribution (helpful when a spike in concentration flattens the color scale for the majority of the time), volume size distribution, and seven hygroscopic growth factor distributions. In the time series figures, the bars colored green, yellow, and red indicate the measurements made at those times were not flagged, were flagged, and were discarded, respectively. The criteria used to identify suspect distributions are provided in Appendix I.

If a 1-week time series is selected a user can click on any of the images to go to the corresponding 1-day page. On the 1-day pages, XY graphs pop-up as the mouse cursor position is moved over the time series. The quantity graphed is controlled through the navigation menu at the far left of the page (it will remain partially hidden until the mouse cursor is moved over it). The default setting is “same as time series”, which will pop-up an XY graph of the quantity in the time series. Thus, if the mouse cursor is positioned over the 200 nm growth factor distribution time series, a graph of the distribution at that time will pop up. For all of the other options, the same graph will appear as the cursor is moved over any time series (at the same time anyway). All of the data shown graphically through the webpage can also be downloaded by clicking on the “txt” links in the calendar. The daily 2-panel back trajectory graphs shown in the calendar in Figure 2 are also available through the webpage.

Study-averaged distributions and complete time series

Study-averaged hygroscopic growth factor distributions are shown in Figure 7. All distributions measured at each site were included when calculating the averages. This approach was selected to maximize the number of distributions included to provide the most representative averages. A disadvantage of the approach is that different data subsets are used for the three sites, precluding exact comparisons. Consistent with almost all measurements our group has made in the Houston area, the hygroscopic growth factor distributions of the smallest particles are monomodal with a hygroscopicity that is frequently intermediate of that of the two modes present in the larger particle measurements. Site-to-site variability in size-resolved properties is rather limited despite the significant differences in local emissions sources. The size-dependent trend in hygroscopicity observed at each of the locations suggests the aerosol is largely an external mixture (multiple particle types present) with the more hygroscopic, sulfate-dominated, mode reaching a peak fractional contribution at roughly 0.2 μm . The similarity among the sites is also apparent in the time-resolved hygroscopic growth factor distributions for Aldine, Bayland Park, and Deer Park shown in Figures 8, 9, and 10, respectively. The time series in the left hand column of each of those figures show the measured hygroscopicity distributions for the project duration. The time series for the 0.6 μm hygroscopicity distributions include all measurements while the others include only those distributions that were not discarded following the automatic QC procedure described in the previous section. The hygroscopic growth distributions of the largest particles are frequently discarded because particle count rates are often insufficient to provide reasonably smooth distributions. Despite the resulting noise in the distributions, the patterns in hygroscopicity are readily apparent in the resulting time series. On the right are study-averaged, time-resolved distributions. Each row represents a different particle size, with the smallest particle (0.013 μm) distributions shown on top and the largest particle (0.6 μm) distributions on bottom. The hygroscopicity of the 0.05 to 0.4 μm diameter particles appears to

vary over timescales sometimes exceeding a day, while that of the smaller particles exhibits little day-to-day variability, instead having a pronounced diurnal pattern that reflects increased importance of sulfuric acid condensation during the afternoon and of secondary organic aerosol at night.

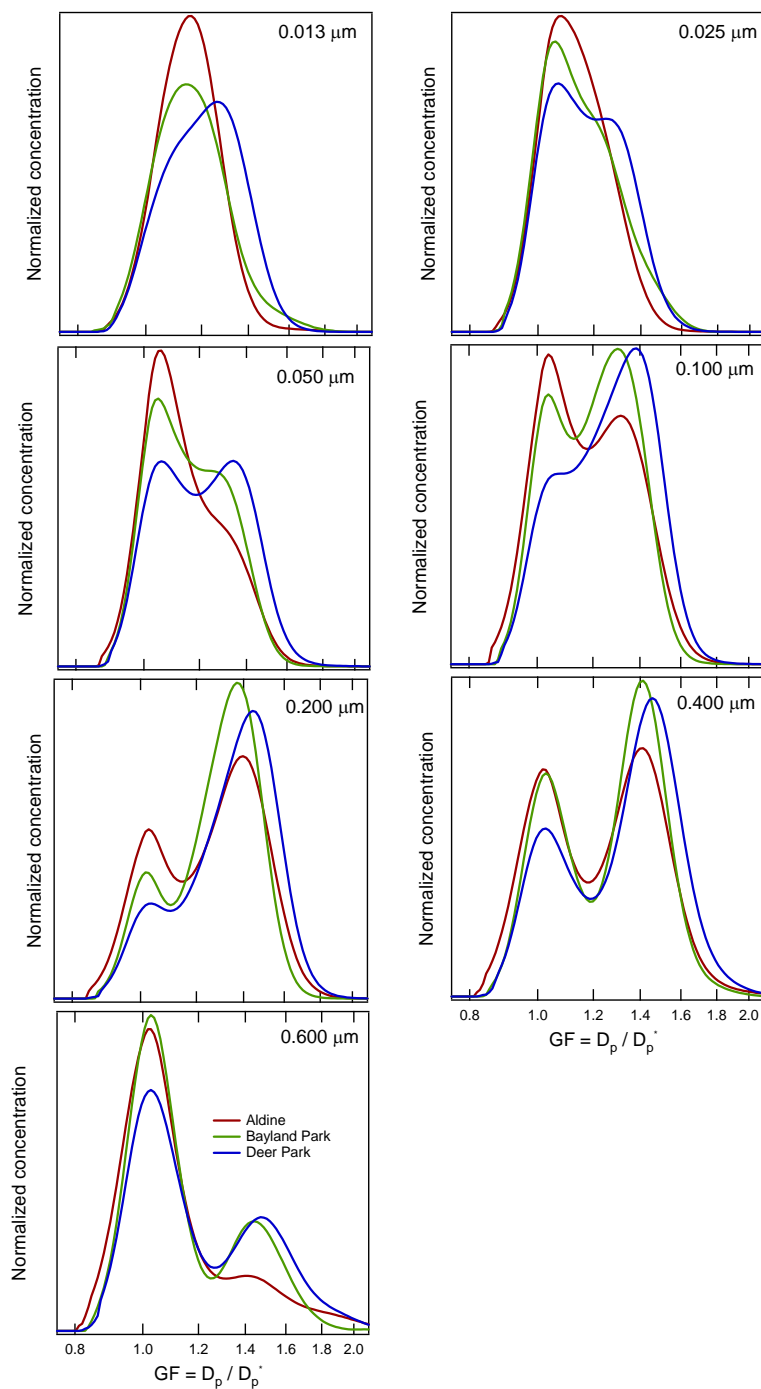


Figure 7. Study-averaged hygroscopic growth factor distributions for each particle size analyzed at each of the three sites.

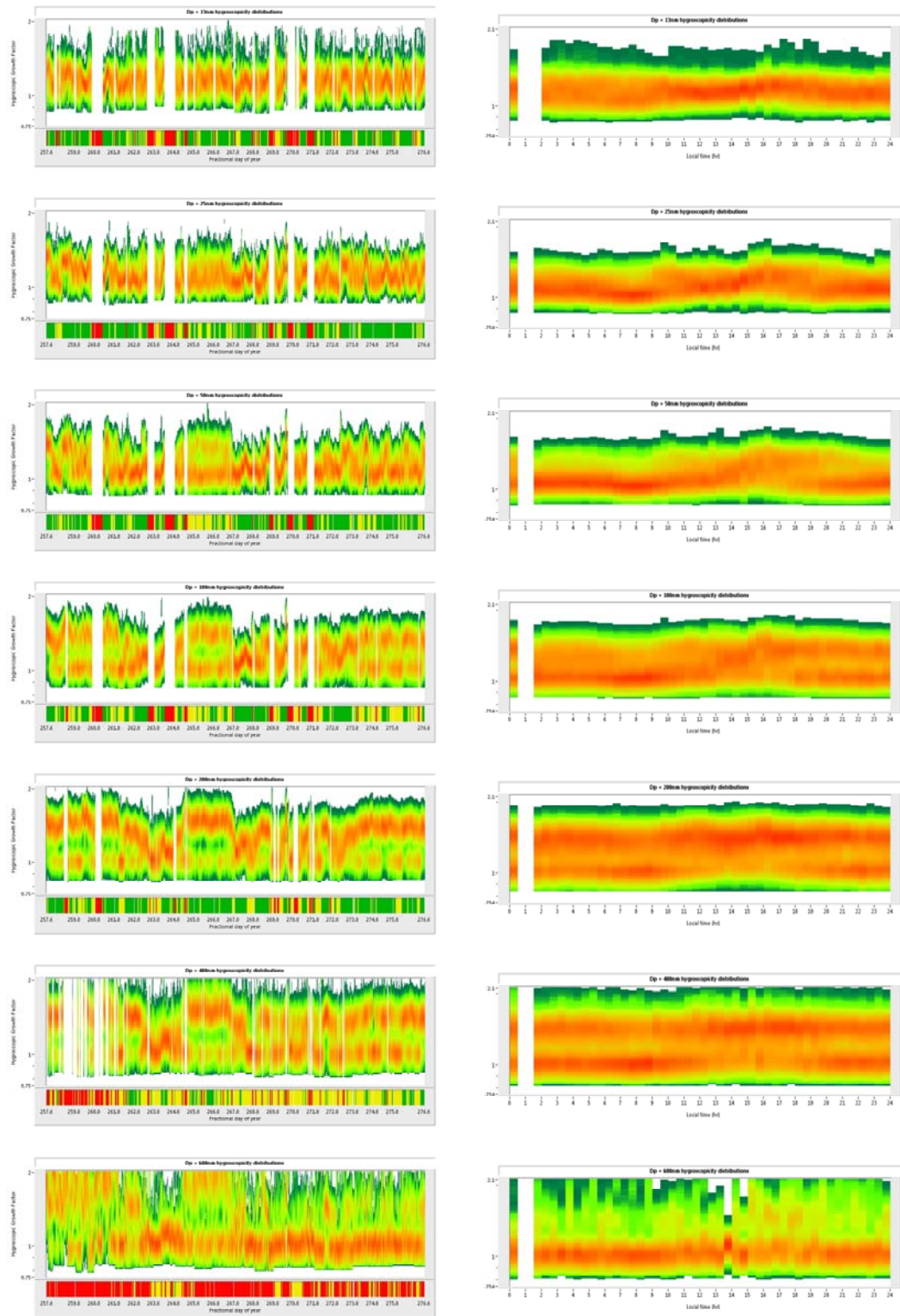


Figure 8. Time-dependent, study-averaged hygroscopic growth factor distributions measured at Aldine. The graphs on the left show time series for the entire project period and those on the right show the study-averaged distributions. The distributions for the smallest particles analyzed ($0.013 \mu\text{m}$) are shown on top and those for the largest particles analyzed ($0.6 \mu\text{m}$) are shown on bottom.

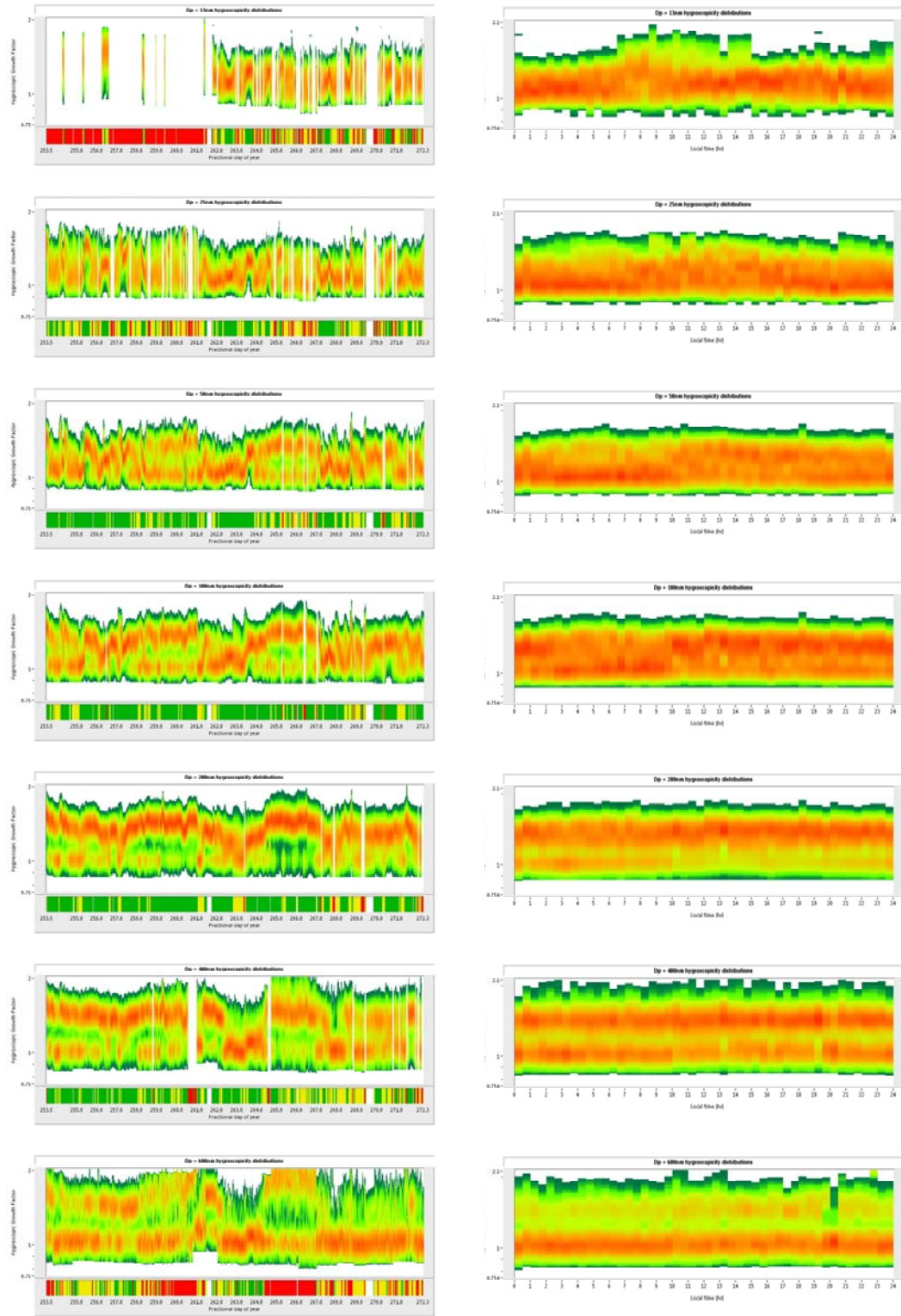


Figure 9. Same as Figure 8 for distributions measured at Bayland Park.

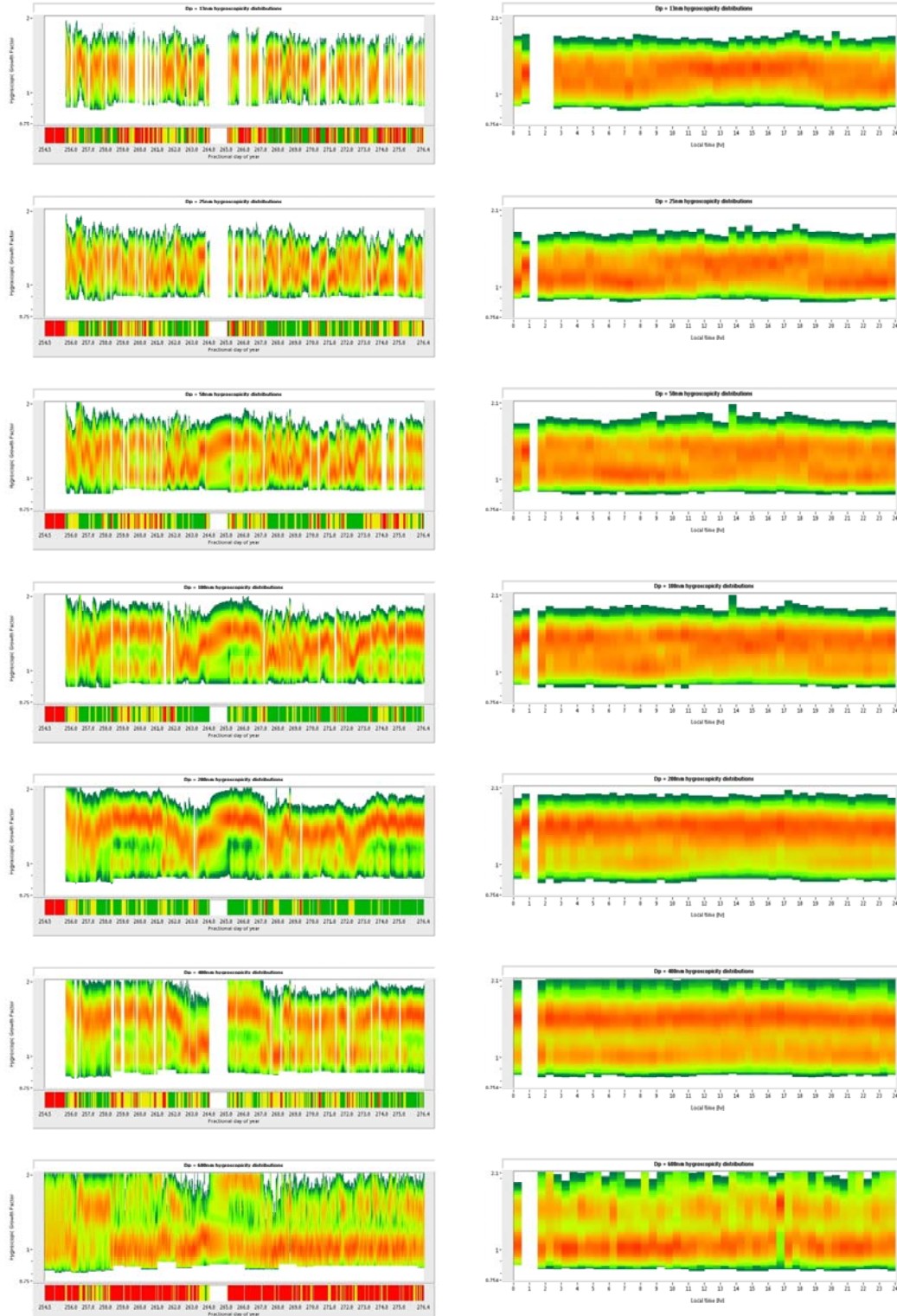


Figure 10. Same as Figure 8 for distributions measured at Deer Park.

Calculated data products

The measured distributions were used to generate a number of products that may be of more direct use by other project participants. These calculated products are presented graphically through the webpage and are also accessible for direct download through the “txt” links. The specific products are as follows:

i) Compositionally-categorized number and mass distributions were generated as they may be most readily compared with compositional measurements such as those made with the aerosol mass spectrometers operated by PNNL. These are calculated by coupling the measured size distributions with size-resolved soluble fraction. The operational definition of the soluble and insoluble components is based only on hygroscopicity as described in Gasparini et al. (2004). During the summer in Houston, the soluble component is dominated by sulfates, while the insoluble component is dominated by organic and elemental carbon for smaller particles and dust for the largest particles measured. In simple terms, categorization of the size-resolved particulate composition is achieved by determining the mass fraction of sulfate required to result in the observed hygroscopicity. Study-averaged compositionally-categorized size distributions for the three sites are shown in Figure 11. The graphs on the left show the categorized number size distributions and those on the right show the categorized mass size distributions. With the exception of the enhanced nucleation mode concentration that was measured at Bayland Park, the distributions have similar shapes. It is important to emphasize that the averaged distributions are not directly comparable because each represents a slightly different averaging period. Time-resolved mass distributions of the soluble and insoluble components are shown in Figure 12. The general features of the distributions measured at the sites are very similar and provide insight into the sources of the distinct components. The impact of mobile emissions of primary aerosols during morning rush hour is evident in the insoluble distributions determined for all three sites. The insoluble particulate concentrations then decrease during the afternoon as the boundary layer depth increases. In contrast, peak concentrations in the soluble size distributions are observed in mid-afternoon during peak photochemical activity. Production of secondary sulfates during this time is pronounced in the number size distributions, but has a relatively modest impact on the resulting mass concentrations. Nevertheless, the small addition of sulfate mass in the urban area can be significant when the background mass concentration is already approaching the NAAQS standard.

ii) The size and hygroscopicity distributions were transformed into distributions describing the size-resolved contribution to RH-dependent light extinction and radar backscattering for direct comparison with optical measurements and for potential use in improving satellite retrievals.

iii) Although the focus of the Houston Triangle project was on local and regional air quality, an objective of the overall TexAQS-II study was to characterize the impact of particulates on climate, with an emphasis on the influence of aerosols on cloud properties. For the benefit of TexAQS-II participants involved in that parallel effort, we also used our measurements to predict the supersaturation-dependent concentration of cloud condensation nuclei.

The data formats and file naming conventions for the text files containing the calculated products are described in Appendix I.

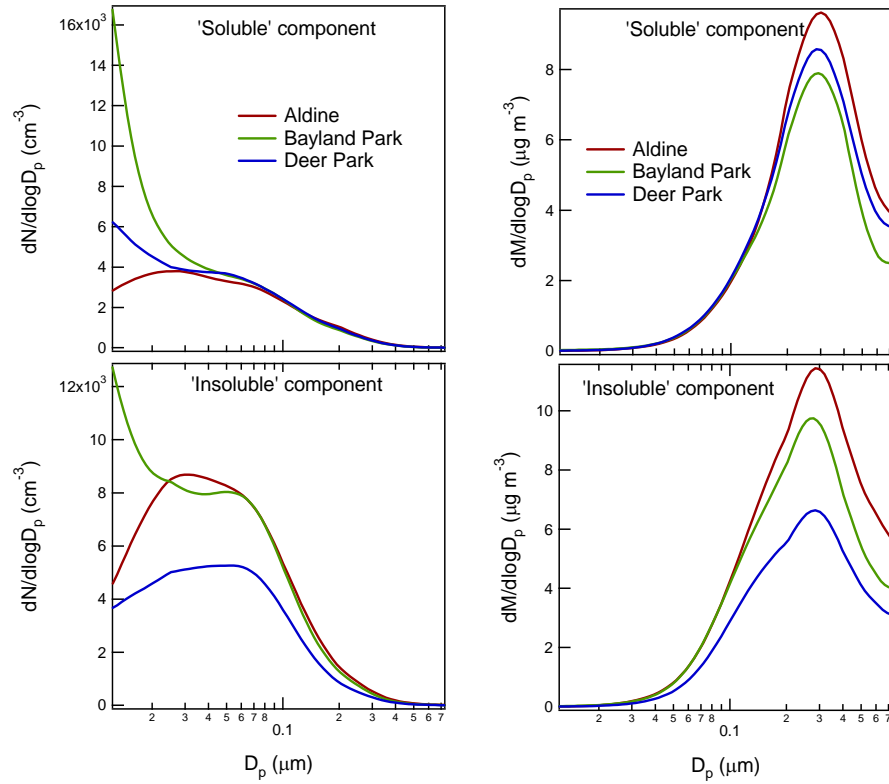


Figure 11. Study-averaged, compositionally-categorized number (left) and mass (right) size distributions.

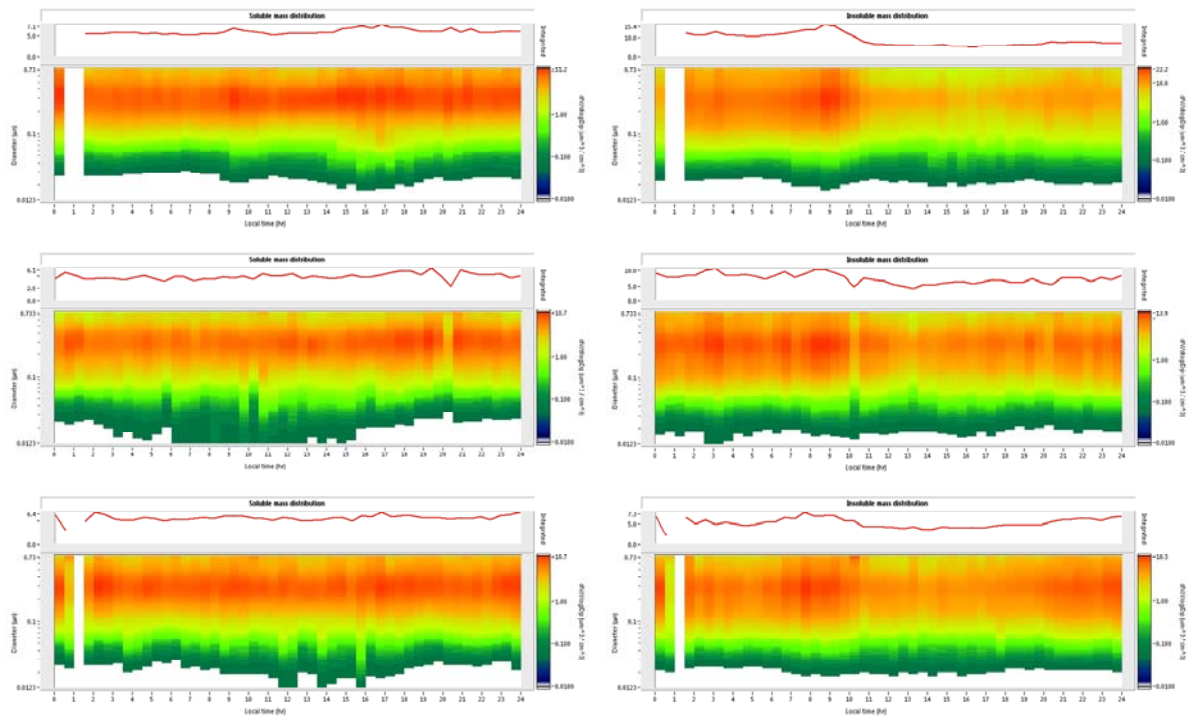


Figure 12. Project average time-dependent, compositionally-resolved mass size distributions.

Comparison of calculated mass concentrations with TCEQ TEOM measurements

To gain confidence in the accuracy of the measured size distributions, mass concentrations calculated by integrating the measured size distributions were compared with direct PM_{2.5} measurements made at the adjacent TCEQ sites. Because PM_{2.5} is not measured at the Bayland Park TCEQ site, only those data collected at the Aldine and Deer Park sites were considered. Comparisons such as these are always complicated by differences in instrument response to varying particle types, differences in the particle size ranges covered, and differences in sampling frequency and integration time. Nevertheless, it is a good way to ensure that no major sources of error impacted the measurements and can often highlight periods of interest that require further attention. Among the reasons the mass concentration reported by TCEQ may differ from that calculated from the size distributions measured with the TDMA's are the following:

- The TEOMs used by TCEQ are used to measure the mass concentration of particles having aerodynamic diameters less than 2.5 μm , while the size range covered using the TDMA extends to particles with electrical mobility diameters of 0.75 μm , which typically corresponds to an aerodynamic diameter of about 1 μm .
- The TEOMs used by TCEQ directly measure mass concentration, while calculation of mass concentration using measured size distributions requires an assumption of particle density (assumed to be 1.5 $\mu\text{g}/\text{m}^3$ here).
- The TEOMs report the average concentration measured each hour, while, because it is used to sequentially measure both size distributions and hygroscopic growth factor distributions, the relevant measurements made with the TDMA span only about 5 minutes and are separated by about 40 minutes.

Despite these potential sources of bias, the two measurements were in rather good agreement. Figure 13 shows the comparisons for Aldine and Deer Park for the period of September 14 – October 3, 2007. The shaded bands highlight a period of interest discussed in the following section.

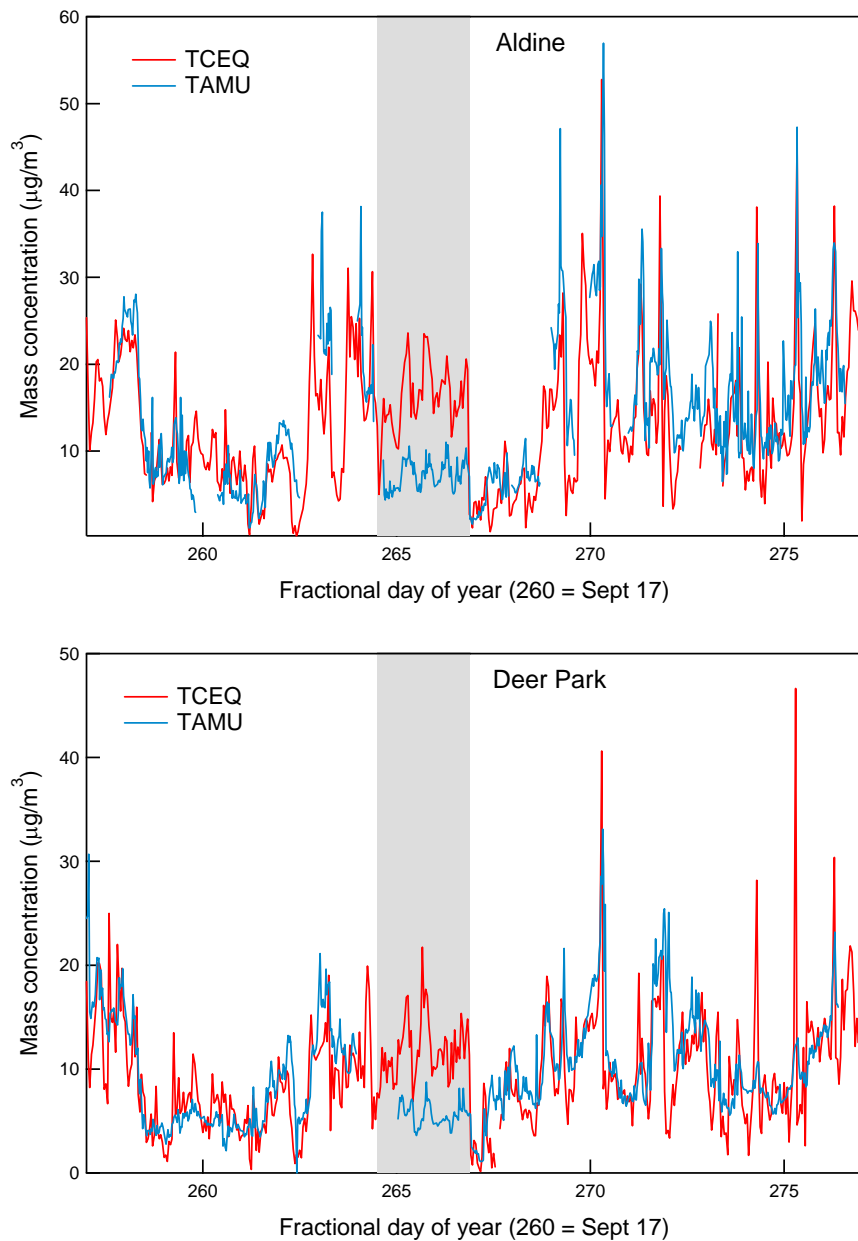


Figure 13. Comparison of particulate mass concentration calculated using the measured size distributions (TAMU) and reported by TCEQ. The relevance of the shaded bands is discussed in the following section.

Evidence of contribution of sea salt to PM_{2.5}

As noted above, there is rather good agreement between the particulate mass concentration calculated using the measured size distributions and that reported by TCEQ throughout most of the 3-week study for both the Deer Park and Aldine sites. However, during the period between September 21 (day 264) and September 24 (day 267), there was an elevated discrepancy between the two. This period is identified in the shaded bands in the mass concentration time series shown in Figure 13.

The disparity between the two is likely explained by an increased contribution to PM_{2.5} by those particles larger than the $\sim 1 \mu\text{m}$ measured using the TDMA. The most likely responsible particle types are dust and sea salt, both of which typically have a supermicron mass median diameter. Interestingly, aerosol model results suggest that a cold front generated a dust plume that reached the Houston area during the early part of highlighted period. As an illustration, the predicted surface dust mass concentration during the morning (local time) of September 21 is shown in Figure 14. The color scale in that figure represents mass concentration of dust in $\mu\text{g}/\text{m}^3$. The modeled concentration in the Houston area was higher during this period than it was at any other time during the Houston Triangle study.

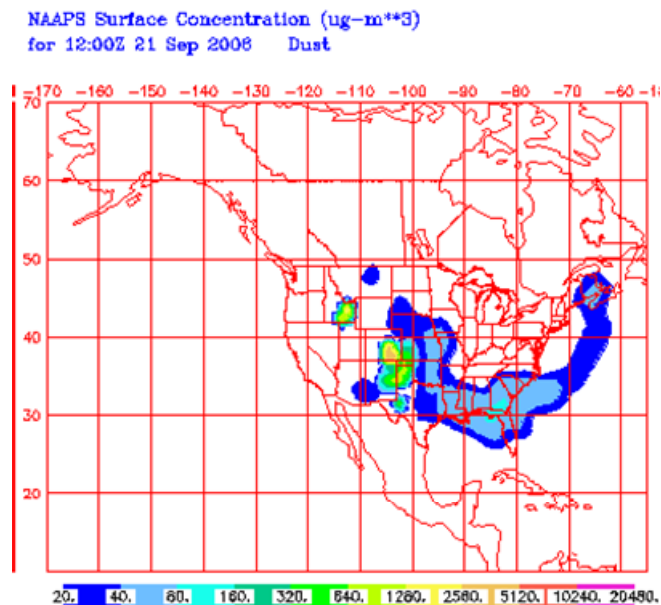


Figure 14. Model forecast surface dust concentration for the beginning of the period of interest.

The $0.6 \mu\text{m}$ hygroscopicity distribution time series included in Figures 8 and 10 are shown again in Figure 15 to highlight the atypical distributions measured during the time interval identified above. It is clear that during the period of interest here the hygroscopicity of the $0.6 \mu\text{m}$ particles is greater than that measured during most of the remainder of the study. Particles composed of dust or primary organics, sulfates or nitrates, and sea salt have growth factors of roughly 1.0, 1.5, and 2.0, respectively, identified as types 1, 2, and 3 in the figure. In contrast to size distributions of primary organics, sulfates, and nitrates, that of sea salt typically has a median exceeding $1.0 \mu\text{m}$. The sea salt particles detected at $0.6 \mu\text{m}$ are at the tail of the distribution, which is why the hygroscopicity mode is barely detectable at $0.4 \mu\text{m}$.

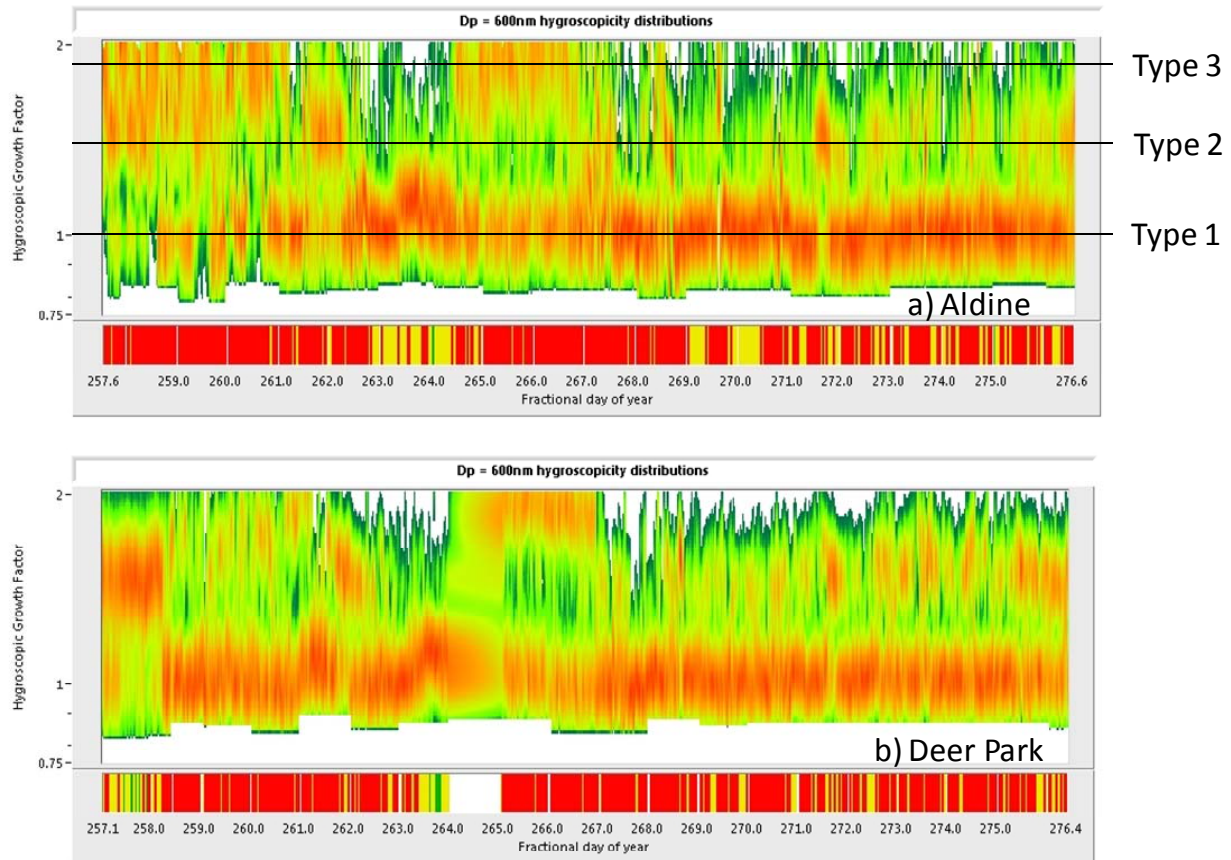
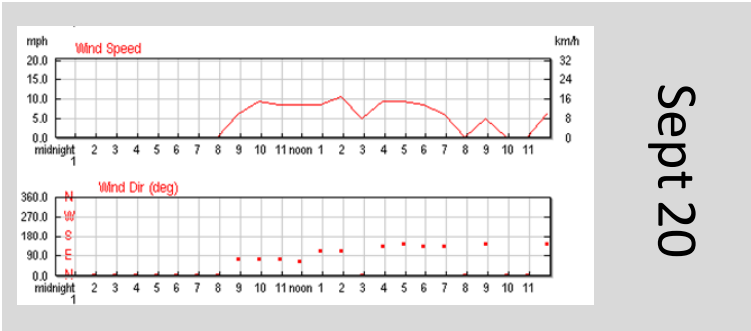
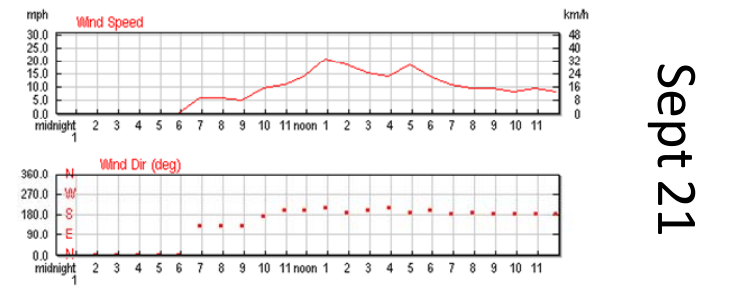


Figure 15. Time series showing the measured hygroscopic growth factor distributions of the largest (0.6 mm) particles analyzed.

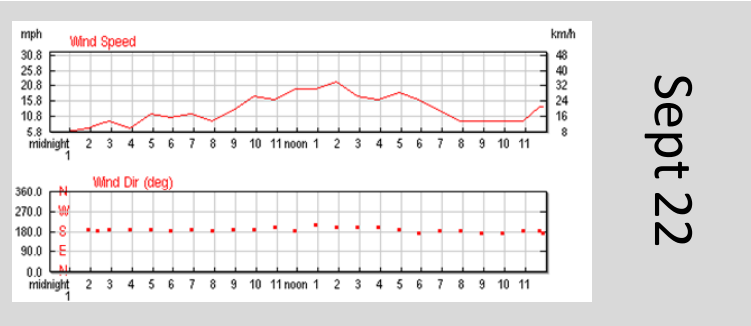
Sea salt production rate is very strongly related to wind speed, as is the efficiency with which the very large and hygroscopic particles can be transported. As expected during periods of elevated sea salt concentration, strong southerly winds were recorded at Houston Hobby throughout this period, which is apparent in Figure 16. As shown that figure, peak wind speed on September 20 was less than 10 mph, while that on September 21, 22, and 23 was roughly 20 mph. Wind speeds were also high on September 24, but the direction shifted from southerly to northerly, effectively shutting off the transport of sea salt from the Gulf. Thus, there is strong evidence that elevated sea salt concentration was responsible for the observed disparity in mass concentrations. During this period, sea salt contributed as much as $15 \mu\text{g}/\text{m}^3$ to the total $\text{PM}_{2.5}$, which emphasizes the importance of this often overlooked particle type in coastal regions.



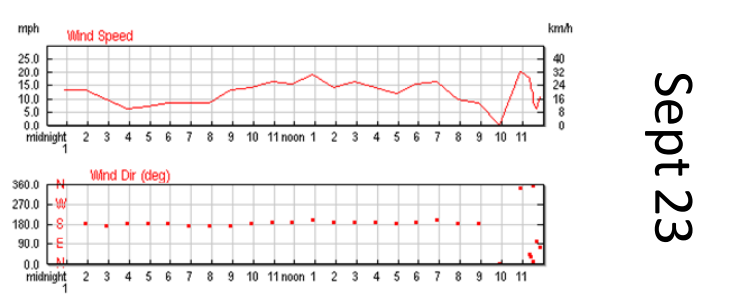
Sept 20



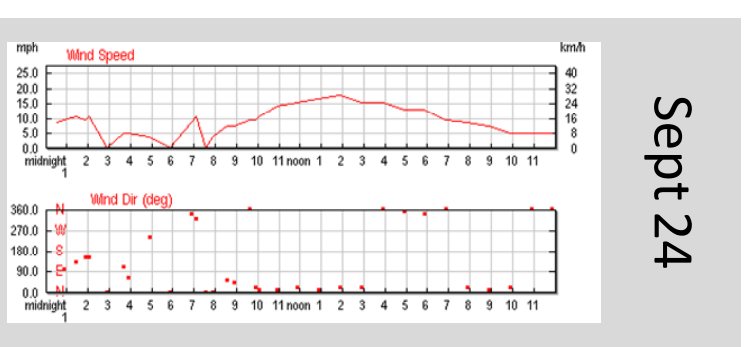
Sept 21



Sept 22



Sept 23



Sept 24

Figure 16. Wind speed and direction recorded at Houston Hobby airport during the time interval of interest here.

Dependence of particulate properties on back trajectory

Despite the brevity of the campaign, the calculated trajectories shown in Figure 2 suggest that air masses of varying origin impacted the study area during the project period. Although there is always variability in particulate composition among the three sites, similar patterns in hygroscopicity were observed on many of the project days. Thus, it is likely that the properties are strongly dependent upon the source region and processing upwind of Houston. During the summer months in Houston, prevailing winds are most frequently from the south. As confirmed by the daily back trajectories, variability in wind direction increases in late summer and early fall when the Houston Triangle project was conducted. Based on those trajectories, the recorded size and hygroscopic growth factor distributions were grouped into four categories: East origin, North origin, South origin, and irregular. No trajectories during the study period originated to the west of Houston. A summary of the categorization is provided in Table 1.

Table 1. Dates for which back trajectories shown in Figure 2 are classified as originating from the north, east, and south.

Origin	Dates
North	Sep 13, 19, 25, 26
East	Sep 14, 15, 20, 29; Oct 3
South	Sep 16, 17, 21, 22, 23, 28, 30; Oct 1, 2
Irregular	Sep 11, 12, 18, 24, 27

Although the trajectory categorization is rather simplistic, differences in the hygroscopicity distributions (which reflect differences in size resolved composition) are discernable in the set of averaged distributions shown in Figure 17. The different colors shown in each of the graphs represent the different particle sizes analyzed as is identified in the color legend on the right of each graph. The vertical lines are used to highlight the difference in hygroscopicity of the larger particles. Specifically, each vertical line is positioned at the peak in the 0.2 μm average hygroscopic growth factor distribution measured when the trajectories were from the north. At each of the three sites, the hygroscopicity of the dominant 0.2 μm diameter particle population was greater when the sampled air came from the south than when from the east, and greater when from the east than from the north. This variation in hygroscopicity likely reflects the organic fraction of these larger particles. Thus, particles originating from north of Houston tend to have a higher organic fraction, and a correspondingly lower sulfate fraction, than those originating south of Houston. It is likely that biogenic emissions from the forests north of Houston may be responsible for additional secondary organic aerosol production that is absent over the Gulf of Mexico. Sulfate produced from oxidation of dimethylsulfide emitted by plankton in the Gulf may also enhance the hygroscopicity of the particles arriving from the south. Interestingly, the hygroscopic growth factor distributions for the 0.6 μm particles indicate a significant and only weakly origin-dependent contribution of dust or some other primary particle type.

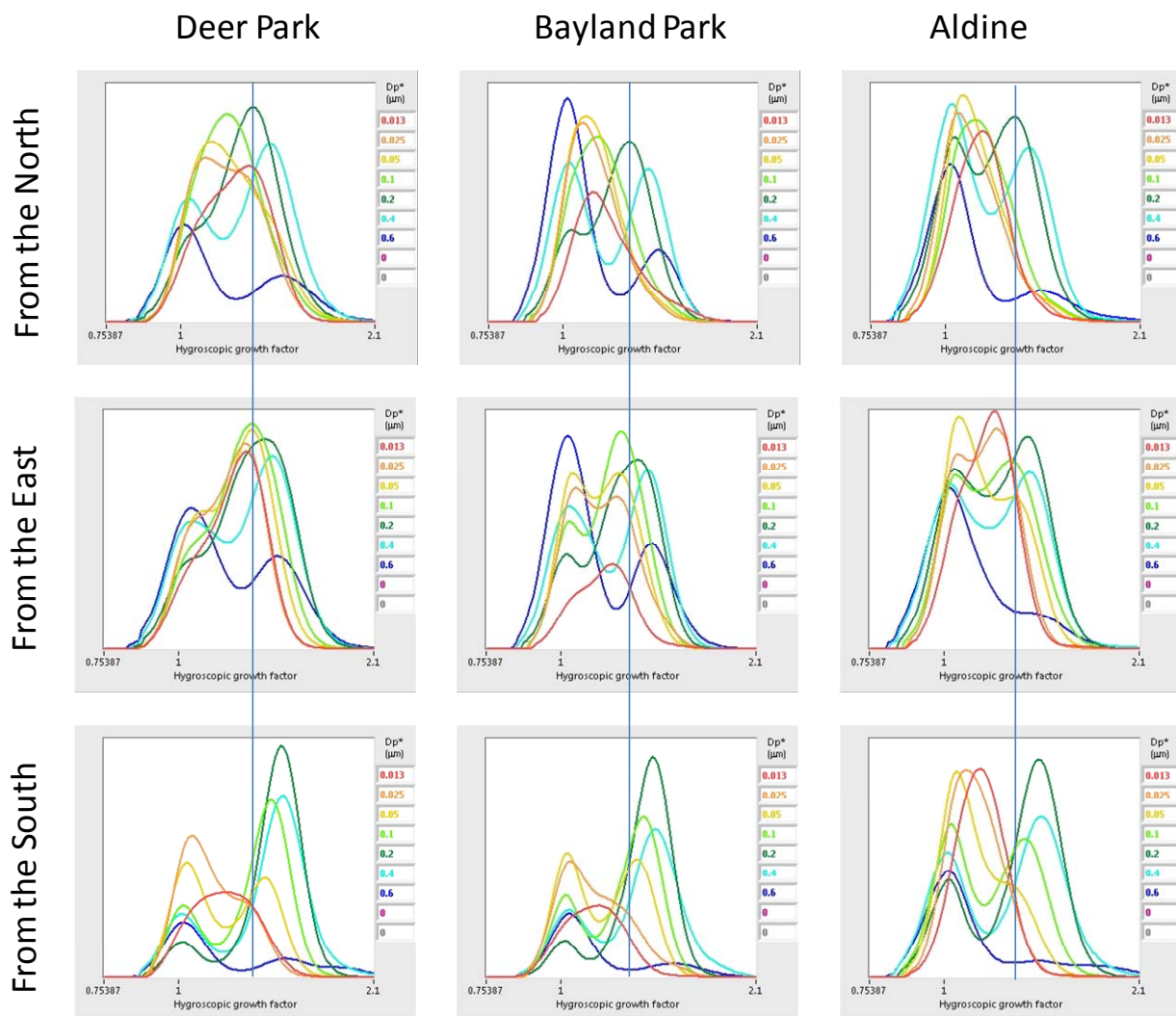


Figure 17. Size-dependent hygroscopic growth factor distributions averaged over the dates identified in Table 1. The colors in each graph correspond to the particle sizes identified in the legends.

References

- Collins, D. R., R. C. Flagan, and J. H. Seinfeld, Improved Inversion of Scanning DMA Data, *Aerosol Science and Technology*, 36, 1-9, 2002.
- Gasparini, R., R. Li, and D. R. Collins, Integration of Size Distributions and Size Resolved Hygroscopicity During the Houston Supersite for Compositional Categorization of the Aerosol, *Atmospheric Environment*, 38, 3285-3303, 2004.
- Gasparini, R., Collins, D. R., Andrews, E., Sheridan, P. J., Ogren, J. A., and Hudson, J. G., 2006. "Coupling aerosol size distributions and size-resolved hygroscopicity to predict humidity-dependent optical properties and CCN spectra," *Journal of Geophysical Research – Atmospheres*, 111, art. No. 6092. Knutson, E. O. and K. T. Whitby, *Aerosol*

Classification by Electric Mobility: Apparatus, Theory, and Applications, *Journal of Aerosol Science*, 6, 443-451, 1975.

Knutson, E. O. and K. T. Whitby, Aerosol Classification by Electric Mobility: Apparatus, Theory, and Applications, *Journal of Aerosol Science*, 6, 443-451, 1975.

Liu, B. Y. H., D. Y. H. Pui, K. T. Whitby, D. B. Kittelson, Y. Kousaka, and R. L. Mckenzie, Aerosol Mobility Chromatograph - New Detector for Sulfuric-Acid Aerosols, *Atmospheric Environment*, 12, 99-104, 1978.

McMurry, P. H. and M. R. Stolzenburg, On the Sensitivity of Particle-Size to Relative-Humidity for Los Angeles Aerosols, *Atmospheric Environment*, 23, 497-507, 1989.

Stolzenburg, M., N. Kreisberg, and S. Hering, Atmospheric Size Distributions Measured by Differential Mobility Optical Particle Size Spectrometry, *Aerosol Science and Technology*, 29, 402-418, 1998.

Appendix I – Formats used in data files

Size distributions file description - mmdyyyy_size_distributions.txt

Data:

Particle Diameters, D_p (μm) -- first row

Time -- first column

Fractional hour

Number Size Distribution -- all rows other than the first

Each value represents the concentration ($dN/d\log D_p; \text{cm}^{-3}$) at the diameter in the same column, measured at the time in the same row

Size distribution flags file description - mmdyyyy_size_distribution_flags.txt

Data:

Time -- first column

Fractional hour

Data quality flags -- columns 2, 3, 4, and 5

A value of 0 indicates no flag

A value of 1 indicates that the distribution is somewhat unusual and may be inaccurate. These distributions are used in the calculated products available in other files.

A value of 2 indicates that the distribution is highly unusual and is likely inaccurate. These distributions are not used in the calculated products available in other files.

Number concentration out of range flag -- column 2

A value of 1 indicates that the integrated number concentration was less than 300 cm^{-3} or greater than $30,000 \text{ cm}^{-3}$.

A value of 2 indicates that the integrated number concentration was less than 100 cm^{-3} or greater than $100,000 \text{ cm}^{-3}$.

Volume concentration out of range flag -- column 3

A value of 1 indicates that the integrated volume concentration was less than $0.5 \mu\text{m}^3/\text{cm}^3$ or greater than $40 \mu\text{m}^3/\text{cm}^3$.

A value of 2 indicates that the integrated volume concentration was less than $0.2 \mu\text{m}^3/\text{cm}^3$ or greater than $80 \mu\text{m}^3/\text{cm}^3$.

Unexpected volume concentration distribution slope flag -- column 4

A value of 1 indicates that the ratio of the differential volume concentrations ($dV/d\log D_p$) at $0.6 \mu\text{m}$ and $0.5 \mu\text{m}$ is greater than 1.0.

A value of 2 indicates that the ratio of the differential volume concentrations ($dV/d\log D_p$) at $0.6 \mu\text{m}$ and $0.5 \mu\text{m}$ is greater than 3.0.

Poor correlation between up and down scan distributions flag -- column 5

A value of 1 indicates that the correlation between the measured up and down scan distributions was less than 0.9.

A value of 2 indicates that the correlation between the measured up and down scan distributions was less than 0.3.

**Hygroscopic growth factor distributions file description -
mmddyymm_##nm_hyg_distributions.txt where ## represents the
particle size in nm**

Data:

Hygroscopic Growth Factors, D_p/D_p^* -- first row

D_p^* -- Initial particle diameter at low (~10%) relative humidity

D_p -- Particle diameter after exposure to elevated (90%) relative humidity

Time -- first column

Fractional hour

Hygroscopic Growth Factor Distribution -- all rows other than the first

Each value represents the (normalized) concentration ($dN/d\log D_p; \text{cm}^{-3}$) at the growth factor in the same column, measured at the time in the same row.

**Hygroscopic growth factor distribution flags file description -
mmddyymm_##nm_hyg_flags.txt where ## represents the particle
size in nm**

Data:

Time -- first column

Fractional hour

Data quality flags -- columns 2, 3, 4, 5, 6, and 7

A value of 0 indicates no flag

A value of 1 indicates the distribution is somewhat unusual and may be inaccurate. These distributions are

used in the calculated products available in other files.

A value of 2 indicates the distribution is highly unusual and is likely inaccurate. These distributions are not used in the calculated products available in other files.

Relative humidity out of range flag -- column 2

A value of 1 indicates that the inter-DMA relative humidity was less than 83% or greater than 93%.

A value of 2 indicates that the inter-DMA relative humidity was less than 78% or greater than 96%.

Excessive number of peaks in distribution flag -- column 3

A value of 1 indicates that the distribution has more than 6 peaks.

A value of 2 indicates that the distribution has more than 9 peaks.

Tails of distribution too high flag -- column 4

A value of 1 indicates that the differential number concentration ($dN/d\log D_p$) at the first or last growth factor bin is greater than 5% of that of the maximum in the distribution.

A value of 2 indicates that the differential number concentration ($dN/d\log D_p$) at the first or last growth factor bin is greater than 15% of that of the maximum in the distribution.

Poor correlation between up and down scan distributions flag -- column 5

A value of 1 indicates that the correlation between the measured up and down scan distributions was less than 0.4.

A value of 2 indicates that the correlation between the measured up and down scan distributions was less than 0.0.

Location of peak in distribution out of range flag -- column 6

A value of 1 indicates that a peak in the distribution was located at a growth factor less than 0.98 or greater than 2.1.

A value of 2 indicates that a peak in the distribution was located at a growth factor less than 0.93 or greater than 2.3.

Insufficient number of particles counted flag -- column 7

A value of 1 indicates that fewer than 15 particles were detected during the measurement.

A value of 2 indicates that fewer than 5 particles were detected during the measurement.

**Calculated low-RH differential extinction coefficient distributions file description -
mmddyymm_low_RH_extinction_distributions.txt**

Data:

Particle Diameters, D_p (μm) -- first row

Time -- first column

Fractional hour

Differential light extinction coefficient distribution -- all rows other than the first

Each value represents the contribution to the overall low-RH (10%) light extinction coefficient ($db_{\text{ext}}/d\log D_p; \text{Mm}^{-1}$) by particles with diameters in the same column, measured at the time in the same row.

**Calculated high-RH differential extinction coefficient distributions file description -
mmddyymm_high_RH_extinction_distributions.txt**

Data:

Particle Diameters, D_p (μm) -- first row

Time -- first column

Fractional hour

Differential light extinction coefficient distribution -- all rows other than the first

Each value represents the contribution to the overall high-RH (90%) light extinction coefficient ($db_{\text{ext}}/d\log D_p$; Mm^{-1}) by particles with dry diameters in the same column, measured at the time in the same row.

**Calculated low-RH differential radar backscattering coefficient distributions file description -
mmddyyyy_low_RH_backscattering_distributions.txt**

Data:

Particle Diameters, D_p (μm) -- first row

Time -- first column

Fractional hour

Differential radar backscattering coefficient distribution -- all rows other than the first

Each value represents the contribution to the overall low-RH (10%) radar backscattering coefficient ($dB_{\text{ext}}/d\log D_p$; $\text{sr}^{-1} \text{Mm}^{-1}$) by particles with diameters in the same column, measured at the time in the same row.

**Calculated high-RH differential radar backscattering coefficient distributions file description -
mmddyyyy_high_RH_backscattering_distributions.txt**

Data:

Particle Diameters, D_p (μm) -- first row

Time -- first column

Fractional hour

Differential radar backscattering coefficient distribution -- all rows other than the first

Each value represents the contribution to the overall high-RH (90%) radar backscattering coefficient

($\text{dB}_{\text{ext}}/\text{dlogD}_p$; $\text{sr}^{-1} \text{Mm}^{-1}$) by particles with dry diameters in the same column, measured at the time in the same row.

**Calculated soluble aerosol number size distributions file
description -
mmddyyyy_soluble_number_distributions.txt**

Data:

Particle Diameters, D_p (μm) -- first row

Time -- first column

Fractional hour

Soluble component number size distribution -- all rows other than the first

Each value represents the concentration (dN/dlogD_p ; cm^{-3}) at the diameter in the same column, measured at the time in the same row. The operational definition of the soluble and insoluble components is based only on hygroscopicity as described in Gasparini et al. (2004). During the summer in Houston, the soluble component is dominated by sulfates, while the insoluble component is dominated by organic and elemental carbon. In simple terms, categorization of the size-resolved particulate composition is achieved by determining the mass fraction of sulfate in the particles required to result in the observed hygroscopicity.

**Calculated insoluble aerosol number size distributions file
description -
mmddyyyy_insoluble_number_distributions.txt**

Data:

Particle Diameters, D_p (μm) -- first row

Time -- first column

Fractional hour

Insoluble component number size distribution -- all rows other than the first

Each value represents the concentration (dN/dlogD_p ; cm^{-3})

at the diameter in the same column, measured at the time in the same row. The operational definition of the soluble and insoluble components is based only on hygroscopicity as described in Gasparini et al. (2004). During the summer in Houston, the soluble component is dominated by sulfates, while the insoluble component is dominated by organic and elemental carbon. In simple terms, categorization of the size-resolved particulate composition is achieved by determining the mass fraction of sulfate in the particles required to result in the observed hygroscopicity.

**Calculated soluble aerosol mass size distributions file description -
mmddyymm_soluble_mass_distributions.txt**

Data:

Particle Diameters, D_p (μm) -- first row

Time -- first column

Fractional hour

Soluble component number size distribution -- all rows other than the first

Each value represents the mass concentration ($dM/d\log D_p$; $\mu\text{g m}^{-3}$) at the diameter in the same column, measured at the time in the same row. The operational definition of the soluble and insoluble components is based only on hygroscopicity as described in Gasparini et al. (2004). During the summer in Houston, the soluble component is dominated by sulfates, while the insoluble component is dominated by organic and elemental carbon. In simple terms, categorization of the size-resolved particulate composition is achieved by determining the mass fraction of sulfate in the particles required to result in the observed hygroscopicity. The soluble component density is assumed to be that of ammonium sulfate and the insoluble component density is assumed to be 1.4 g/cm^3 .

**Calculated cumulative CCN spectra file description -
mmddyymm_cumulative_CCN.txt**

Data:

Critical supersaturation, S_c (%) -- first row

Time -- first column

Fractional hour

Cumulative CCN distribution -- all rows other than the first

Each value represents the expected CCN concentration (cm^{-3}) at the supersaturation in the same column, based on the size and hygroscopicity distributions measured at the time in the same row. A description of the technique used is provided in Gasparini et al. (2006).

**Calculated differential CCN spectra file description -
mmddyyyy_differential_CCN.txt**

Data:

Critical supersaturation, S_c (%) -- first row

Time -- first column

Fractional hour

Differential CCN distribution -- all rows other than the first

Each value represents the expected CCN concentration ($dN/d\log S_c; \text{cm}^{-3}$) at the critical supersaturation in the same column, based on the size and hygroscopicity distributions measured at the time in the same row. A description of the technique used is provided in Gasparini et al. (2006).